Cooling Limits for GaN HEMT Technology

Yoonjin Won*, Jungwan Cho*, Damena Agonafer, Mehdi Asheghi, and Kenneth E. Goodson

Mechanical Engineering Department, Stanford University, Stanford, CA 94305

***Abstract* — The peak power density of GaN HEMT technology is limited by a hierarchy of thermal resistances from the junction to the ambient. Here we explore the ultimate or *fundamental* cooling limits made possible by advanced thermal management technologies including GaN-diamond composites and nanoengineered heat sinks. Through continued attention to near-junction resistances and extreme flux convection, power densities that may exceed 50 kW/cm^2 – depending on gate width and hotspot dimension – are feasible within 5 years.**

***Keywords* — GaN, HEMT, Electronics Cooling**

I. Introduction

Recent progress on electronics thermal management has been motivated in part by the increasing power densities in microprocessors [1], power semiconductor lasers, and radar amplifiers [2], [3]. GaN high-electron-mobility transistor (HEMT) technology has received special attention due to the limits posed by thermal resistances at the device, substrate, package, and system levels [4]-[6]. Companies will select advanced HEMT cooling technologies for applications in aircraft, satellites, and land vehicles by balancing materials and manufacturing costs against improved performance. The complexity of this balance has overshadowed the recent extensions of the *fundamental* cooling limits, i.e., the increases in peak power density that are becoming feasible independent of system level and cost concerns.

Here we examine the fundamental thermal resistance limits in two parts: Conduction/spreading in composite substrates (electron kinetic energy in the transistor is converted to phonons and then spread by conduction) and fluidic convection in advanced heat sinks (from phonons to the working fluid). We consider the state of the art of both of these technologies, and project advancements through this decade and beyond. This includes a review of recent DARPA-sponsored progress on the translation of electron kinetic energy in GaN HEMTs to phonons in a high conductivity substrate (NJTT [6]), and then to fluid enthalpy through nanoengineered heat sinks (ICECool Fundamentals). This trajectory of energy carrying mechanisms dictates the *fundamental* cooling limit, which assumes an arbitrarily large and expensive heat rejection apparatus to the ambient air. The best combination of junction-level and heat-sink level cooling requires optimization considering spreading, and we quantify this relationship with 3D finite element simulations.

II. Review of Composite Substrate Technologies

Any effort to minimize thermal resistance must aggressively spread heat near the junction. Composite substrates made from diamond can offer local thermal conductivities higher by an order of magnitude compared with GaN and by a factor of nearly 4 compared with SiC [7]-[9]. But the much larger lattice mismatch between GaN and diamond (11%) compared with that between GaN and SiC (3.5%) makes diamond integration very challenging, with existing techniques yielding large defect concentrations or fully amorphous regions that impair heat conduction cooling of the junction.

Prior work used AlGaN/GaN heterostructures grown on (111) single-crystal diamond substrates using molecular beam epitaxy (MBE) [10] and metal-organic chemical vapor deposition (MOCVD) [11] with transition layers of thickness near 500 nm to mitigate the lattice mismatch. Epitaxial transfer [12] was used to attach MOCVD-grown AlGaN/GaN to diamond using disordered film thinner than 50 nm. The interface thermal resistance for this approach is governed by that of the disordered layer as well as the near-interfacial diamond [13].

Figure 1 depicts the mechanisms responsible for the GaN-diamond interface resistance: a) Phonon scattering at

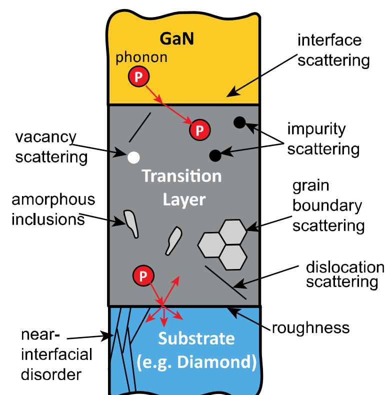

Fig. 1. Mechanisms governing the interface thermal resistance in composite GaN substrates. At present the resistance is governed by thermal resistances associated with material disorder rather than discrete phonon scattering at interfaces.

* These authors contributed equally to this work.

978-1-4799-0583-6/13/$31.00 ©2013 IEEE

TABLE I

GaN-Substrate Thermal Interface Resistances Summary

Article	Measurement Technique	Configuration	Temp. Range	Transition Layer Thickness [nm]	$R_{GaN\text{-}Substrate}$ [m^2K/GW]	DMM prediction [m^2K/GW]
Sarua *et al*. [9] (2007)	Micro Raman Thermometry	GaN-Si	573 K	N/A	33	0.8
Cho *et al*. [8] (2013)	Time-domain Thermoreflectance	GaN-Si	300 to 550 K	38	7−10	0.8
Monoi *et al*. [14] (2010)	Micro Raman Thermometry	GaN-SiC	330 to 520 K	40−200	8−60	1.1
Cho *et al*. [8], [15] (2012, 2013)	Time-domain Thermoreflectance	GaN-SiC	300 to 550 K	26−36	4−7	1.1
Kuzmik *et al*. [16] (2011)	Transient Interferometric Mapping	GaN-Diamond	Room Temp.	N/A	< 10	3.0
Cho *et al*. [13] (2013)	Time-domain Thermoreflectance	GaN-Diamond	Room Temp.	145−324	36−47	3.0

the transition layer boundaries with GaN and the substrate, b) scattering on point defects, dislocations and other defects, and c) scattering by near-interfacial disorder in the GaN and substrate. These contributions are lumped and represented as a single effective interface resistance.

Table 1 summarizes interface thermal resistance data for GaN-Si, GaN-SiC, and GaN-diamond composites with theoretical lower limits at room temperature predicted by the diffuse mismatch model (DMM) [17], [18]. Temperature fields obtained with micro Raman thermometry were used to extract MOCVD GaN-SiC and GaN-Si interface resistances [9], [14], yielding relatively large thermal resistances that varied rapidly with temperature between 330 and 520K. Transient interferometric mapping (TIM) estimated interface resistances of 120 m^2K/GW (± 50%) for MOCVD GaN-SiC [19] and 10 m^2K/GW for GaN on single crystalline diamond [16]. These approximate measurements did not extract the GaN properties independently.

Time-domain thermoreflectance (TDTR) on multiple GaN thicknesses was used to extract both the GaN thermal conductivity and the GaN-substrate thermal interface resistance [8], [15], yielding lower resistances (with weaker temperature dependences) than those reported in [14]. Phonon transport arguments suggest that point defect scattering near the AlN interfaces with the adjacent GaN and SiC (or Si) dominates the resistance [8]. TDTR on two GaN-AlGaN-diamond composites fabricated using epitaxial transfer [12] yielded interface resistances of 36-47 m^2K/GW at 300K [13] and suggested the possibility of ~30 m^2K/GW through further etching of the transition material. With continued fabrication effort, the GaN-diamond interface resistance may fall well below 10 m^2K/GW within the next 5 years, at which point there will be substantive advantages relative to GaN-SiC [13].

III. Convection Resistances in Advanced Heat Sinks

The last three decades brought a revolution in the power densities managed using compact heat exchangers and micro heat sinks [20]-[22]. Tuckerman and Pease [23] demonstrated a microchannel heat sink with thermal resistance of 0.9 cm^2K/W using liquid water, and much subsequent effort has examined the possibility of reduced flowrates and potentially higher heat transfer coefficients using convective boiling. Two-phase flow is promising for reducing pumping power requirements, but convection in long channels can introduce Ledinegg instabilities, flow regime oscillation, and dryout/hotspots [24]-[26].

Much effort has been invested in advanced fluid routing and manifolding methodologies that decrease pressure drop for single-phase flow and improve stability for two-phase flows [27], [28]. The fluid routing challenge was addressed through tree-like or fractal-derived networks [29], [30] or through distributed chip-normal manifolding [31]. Several patents feature distributed, chip-normal fluid routing to a microfluidic heat exchange region [32], [33], which could take the form of either microchannels, distributed microscale pin fins, or microporous foam. All of these studies reduce the axial length over which fluid must traverse the narrowest regions of the heat exchanger.

Nanoengineered structures and surfaces that can be integrated into liquid-vapor phase change systems have revolutionized the design of heat sinks. David *et al*. [28] demonstrated vapor removal through a porous hydrophobic membrane considering both pressure drop and thermal resistance. Thin-layer evaporative cooling devices integrated with nanoporous alumina structures have achieved heat removal up to 600 W/cm^2 [34].

TABLE 2

COMPARISON BETWEEN COMPETING COOLING TECHNOLOGIES

Article	Phase	Technology	Heat Removal (W/cm^2)
Prasher *et al*. [35] (2005)	Single-phase	Microchannel	1250
Kosar *et al*. [36] (2005)	Two-phase	Microchannel	400
Weibel, *et al*. [37] (2012)	Two-phase	Nanostructures	500
David *et al*. [28] (2011)	Two-phase	Channel with vapor escaper	82
Narayan *et al*. [34] (2010)	Two-phase	Nanostructures	600

Nanostructured surfaces may change the wetting characteristics and potentially enhance transport phenomena at micro/nano scales. Superhydrophobic surfaces [38], hydrophobic-hydrophilic patterns [39], and the use of micro/nanoengineered features [40] can promote spontaneous bubble removal and assist heat removal from the surface. Continued attention to nanoengineered surface features is expected to continue the trends to higher heat fluxes and improved stability.

Table 2 summarizes convection flux results for single- and two-phase flow. Single-phase cooling has been demonstrated up to 1 kW/cm^2 in microchannels [35], although higher levels are certainly feasible. Two-phase flow boiling has been demonstrated at 400 W/cm^2 in microchannels [36] and 600 W/cm^2 integrated with nanoporous alumina membranes [34].

IV. RESULTS AND DISCUSSION

Sections II and III summarize progress on reducing thermal resistances due to conduction in the substrate and convection into the working fluid. While progress on these two mechanisms has been performed independently, the peak cooling performance relies on their combination and interactive optimization for a given lateral cooling area. To track and examine this interaction, finite element simulations are used here to account for the thermal resistance associated with the GaN and transition layer and conduction within a chip (SiC or diamond) and a spreader (copper or diamond). All of the simulations use a hotspot with lateral dimensions of 125 μm × 400 μm. We perform these simulations starting with a baseline resembling contemporary practice and extend to designs containing advanced materials and heat sink strategies in future years. Our solution features either copper fins or a porous copper layer for heat exchange with either single-phase or two-phase flow. While single- and two-phase convection yield comparable thermal resistance, there is a substantial difference in required flowrate and pressure drop. Multiple layers from junction

to convecting fluid in simulation models are shown in Fig 2a. For the baseline cooling strategy, we integrate GaN (1 μm), a transition layer (40 nm), SiC (100 μm),

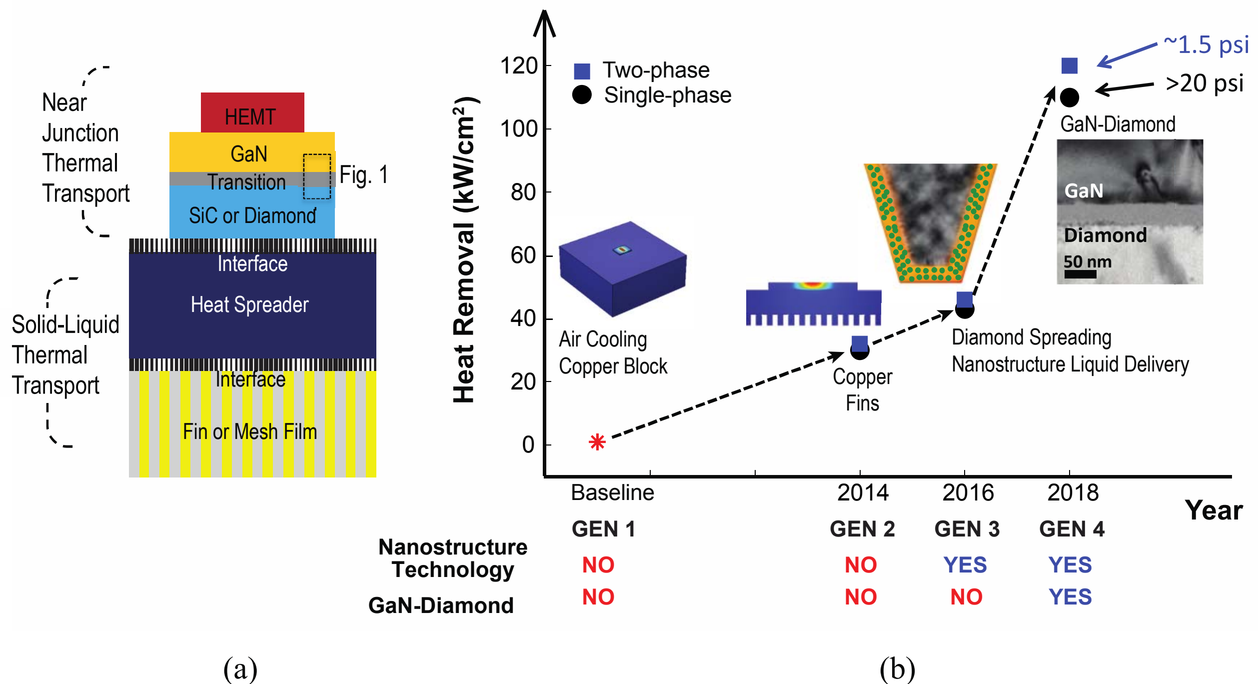

(a) (b)

Fig 2. (a) Configurations of multiple layers from junction to convecting fluid in simulation models to account for near junction thermal transport and solid-liquid convection, which together dictate a fundamental limit for GaN HEMT thermal management. (b) Maximum heat fluxes of hotspots for a baseline model and advanced thermal solutions when junction temperature is maintained at 100°C.

indium (20 μm), and a copper spreader (200 μm). We use a heat transfer coefficient, h, of 100 W/m^2-K for air-cooling and thermal resistance of 20 m^{2}K/GW for the transition layer. The baseline structure removes a heat flux of 1 kW/cm^2 with hotspot temperature maintained at 100°C, as indicated in Fig 2b. For the generation 2 structure, we use a thinner layer of SiC (50 μm) and attach copper fins with a height of 100 μm to the bottom. A single-phase heat transfer coefficient can be estimated using $h \sim Nuk/(w/2)$ for laminar flow (Nu=4), where k is the thermal conductivity of the liquid film, and w is the width of channel (20 μm). This yields h of 50 kW/m^2-K and 100 kW/m^2-K for single-phase and two-phase heat sinks. The copper fins achieve a heat flux of 20 kW/cm^2 when the hotspot temperature is maintained at 100°C. For the generation 3 structure, to reduce the total thermal resistance of the heat sinks, we replace the copper spreader and fins (400 W/m-K) with a diamond spreader (2,000 W/m-K) and micro porous copper [41]. This design will access the higher conductivity of diamond, enabling the effective values of h to be estimated as 100 kW/m^2-K and 200 kW/m^2-K. The integration of a diamond substrate and micro porous copper increases the maximum heat removal by a factor of 2 from the design with copper fins. For the generation 4 structure, to raise the cooling limit again, the GaN structure is directly attached to the diamond substrate, and this significantly decreases the total thermal resistances. The combined technologies of diamond spreading, micro/nano structures, and GaN-diamond composite result in removal of heat fluxes in excess of 100 kW/cm^2, which shows much better performance than the baseline model. Two-phase convection in porous structures enhances heat transfer performance by obtaining a stable, ultra-thin evaporating liquid film at the walls of the heat exchanger that remains wetted even at extreme heat fluxes. Complex design, for example, associated with the vapor phase extraction can achieve very small pressure drop.

V. Concluding Remarks

Here we review both composite substrate and advanced heat sink technologies and project advancements that will facilitate GaN HEMT cooling in the next 5 years. GaN-diamond composites will enhance the near-junction cooling owing to recent reductions in the GaN-diamond interface resistance and improvement in the quality of near-interfacial diamond. Micro and nanostructured heat sinks will improve convection resistance by leveraging a variety of technologies including diamond fin walls an micro/nano-porous phase change media. The rapid development of both conduction and convection technologies will raise the cooling limits of GaN HEMT devices to 50 kW/cm^2 within the next 5 years and the eventual possibility of 100+ kW/cm^2. Realization of these extreme levels of performance will rely on progress in ambient heat rejection, which is highly application specific and not addressed here.

Acknowledgment

The authors acknowledge support from AFOSR and DARPA MTO under NJTT and ICECool programs, as well as collaboration and direct sponsorship from Raytheon, BAE Systems, RFMD, Group4 Labs.

References

[1] S.-C. Lin and K. Banerjee, “Cool chips: Opportunities and implications for power and thermal management,” Electron Devices, IEEE Transactions on, vol. 55, no. 1, pp. 245–255, 2008.

[2] S. Kumar, “Recent Progress in Terahertz Quantum Cascade Lasers,” IEEE J. Select. Topics Quantum Electron., vol. 17, no. 1, pp. 38–47, 2011.

[3] U. K. Mishra, Shen Likun, T. E. Kazior, and Yi-Feng Wu, “GaN-Based RF Power Devices and Amplifiers,” Proceedings of the IEEE, vol. 96, no. 2, pp. 287–305, 2008.

[4] S. V. Garimella, A. S. Fleischer, J. Y. Murthy, A. Keshavarzi, R. Prasher, C. Patel, S. H. Bhavnani, R. Venkatasubramanian, R. Mahajan, Y. Joshi, B. Sammakia, B. A. Myers, L. Chorosinski, M. Baelmans, P. Sathyamurthy, and P. E. Raad, “Thermal challenges in next-generation electronic systems,” Components and Packaging Technologies, vol. 31, no. 4, pp. 801–815, 2008.

[5] K. P. Bloschock and A. Bar-Cohen, “Advanced thermal management technologies for defense electronics,” Proc of SPIE Vol, 2012.

[6] A. Bar-Cohen, J. D. Albrecht, and J. J. Maurer, “Near-Junction Thermal Management for Wide Bandgap Devices,” presented at the 2011 IEEE Compound Semiconductor Integrated Circuit Symposium (CSICS), 2011, pp. 1–5.

[7] J. E. Graebner, “Measurements of specific heat and mass density in CVD diamond,” Diamond and Related Materials, vol. 5, no. 11, pp. 1366–1370, Nov. 1996.

[8] J. Cho, Y. Li, W. E. Hoke, D. H. Altman, M. Asheghi, and K. E. Goodson, “Phonon scattering in strained transition layers for GaN heteroepitaxy,” submitted and under review, May 2013.

[9] A. Sarua, H. Ji, K. P. Hilton, D. J. Wallis, M. J. Uren, T. Martin, and M. Kuball, “Thermal boundary resistance between GaN and substrate in AlGaN/GaN electronic devices,” Electron Devices, IEEE Transactions on, vol. 54, no. 12, pp. 3152–3158, 2007.

[10] M. Alomari, A. Dussaigne, D. Martin, N. Grandjean, C. Gaquière, and E. Kohn, “AlGaN/GaN HEMT on (111) single crystalline diamond,” Electron. Lett., vol. 46, no. 4, pp. 299–301, 2010.

[11] K. Hirama, M. Kasu, and Y. Taniyasu, “RF High-Power Operation of AlGaN/GaN HEMTs Epitaxially Grown on Diamond,” Electron Device Letters, IEEE, vol. 33, no. 4, pp. 513–515, 2012.

[12] D. Francis, F. Faili, D. Babić, F. Ejeckam, A. Nurmikko, and H. Maris, “Formation and characterization of 4-inch GaN-on-diamond substrates,” Diamond and Related Materials, vol. 19, no. 2, pp. 229–233, Feb. 2010.

[13] J. Cho, Z. Li, E. Bozorg-Grayeli, T. Kodama, D. Francis, F. Ejeckam, F. Faili, M. Asheghi, and K. E. Goodson, “Improved

Thermal Interfaces of GaN-Diamond Composite Substrates for HEMT Applications," IEEE Trans. on Components, Packaging and Manufacting Technology, vol. 3, no. 1, pp. 79–85, Jan. 2013.

[14] A. Manoi, J. W. Pomeroy, N. Killat, and M. Kuball, "Benchmarking of thermal boundary resistance in AlGaN/GaN HEMTs on SiC substrates: Implications of the nucleation layer microstructure," Electron Device Letters, IEEE, vol. 31, no. 12, pp. 1395–1397, 2010.

[15] J. Cho, E. Bozorg-Grayeli, D. H. Altman, M. Asheghi, and K. E. Goodson, "Low thermal resistances at GaN–SiC interfaces for HEMT technology," Electron Device Letters, IEEE, vol. 33, no. 3, pp. 378–380, 2012.

[16] J. Kuzmík, S. Bychikhin, D. Pogany, E. Pichonat, O. Lancry, C. Gaquière, G. Tsiakatouras, G. Deligeorgis, and A. Georgakilas, "Thermal characterization of MBE-grown GaN/AlGaN/GaN device on single crystalline diamond," Journal of Applied Physics, vol. 109, no. 8, pp. 086106–086106–3, 2011.

[17] E. Swartz and R. Pohl, "Thermal boundary resistance," Reviews of Modern Physics, vol. 61, no. 3, pp. 605–668, Jul. 1989.

[18] L. D. Bellis, P. E. Phelan, and R. S. Prasher, "Variations of acoustic and diffuse mismatch models in predicting thermal-boundary resistance," Journal of thermophysics and heat transfer, vol. 14, no. 2, pp. 144–150, 2000.

[19] J. Kuzmík, S. Bychikhin, D. Pogany, C. Gaquière, E. Pichonat, and E. Morvan, "Investigation of the thermal boundary resistance at the III-Nitride/substrate interface using optical methods," Journal of Applied Physics, vol. 101, no. 5, pp. 054508–054508–6, 2007.

[20] B. Agostini, M. Fabbri, J. E. Park, L. Wojtan, J. R. Thome, and B. Michel, "State of the Art of High Heat Flux Cooling Technologies," Heat Transfer Engineering, vol. 28, no. 4, pp. 258–281, Apr. 2007.

[21] S. G. Kandlikar, "High Flux Heat Removal with Microchannels—A Roadmap of Challenges and Opportunities," Heat Transfer Engineering, vol. 26, no. 8, pp. 5–14, Oct. 2005.

[22] C. B. Sobhan and S. V. Garimella, "A COMPARATIVE ANALYSIS OF STUDIES ON HEAT TRANSFER AND FLUID FLOW IN MICROCHANNELS," Microscale Thermophysical Engineering, vol. 5, no. 4, pp. 293–311, Oct. 2001.

[23] D. Tuckerman and R. Pease, "High-performance heat sinking for VLSI," IEEE Electron Device Letters, vol. 2, no. 5, pp. 126–129, 1981.

[24] L. Zhang, J. M. Koo, L. Jiang, M. Asheghi, and K. E. Goodson, "Measurements and Modeling of Two-Phase Flow in Microchannels With Nearly Constant Heat Flux Boundary Conditions," Journal of Microelectromechanical Systems, vol. 11, no. 1, pp. 12–19.

[25] S. G. Kandlikar, "History, advances, and challenges in liquid flow and flow boiling heat transfer in microchannels: A critical review," Transactions of the ASME-C-Journal of HeatTransfer, vol. 134, no. 3, p. 034001, 2010.

[26] L. Lin, A. Pisano, and V. Carey, "Thermal bubble formation on polysilicon micro resistors," Journal of Heat Transfer, 1998.

[27] E. G. Colgan, B. Furman, A. Gaynes, W. Graham, N. LaBianca, J. H. Magerlein, R. J. Polastre, M. B. Rothwell, R. J. Bezama, and R. Choudhary, "A practical implementation of silicon microchannel coolers for high power chips," 21st IEEE SEMI-THERM Symposium, pp. 1–7, 2005.

[28] M. P. David, J. Miler, J. E. Steinbrenner, Y. Yang, M. Touzelbaev, and K. E. Goodson, "Hydraulic and thermal characteristics of a vapor venting two-phase microchannel heat exchanger," International Journal of Heat and Mass Transfer, vol. 54, no. 25, pp. 5504–5516, Dec. 2011.

[29] S. M. Senn and D. Poulikakos, "Laminar mixing, heat transfer and pressure drop in tree-like microchannel nets and their application for thermal management in polymer electrolyte fuel cells," Journal of Power Sources, vol. 130, no. 1, pp. 178–191, May 2004.

[30] W. Escher, B. Michel, and D. Poulikakos, "Efficiency of optimized bifurcating tree-like and parallel microchannel networks in the cooling of electronics," International Journal of Heat and Mass Transfer, vol. 52, no. 5, pp. 1421–1430, Feb. 2009.

[31] T. Baummer, E. Cetegen, M. Ohadi, and S. Dessiatoun, "Force-fed evaporation and condensation utilizing advanced micro-structured surfaces and micro-channels," Microelectronics Journal, vol. 39, no. 7, pp. 975–980, Jul. 2008.

[32] T. W. Kenny, M. Munch, P. Zhou, and J. G. Shook, "Patent US6988534 - Method and apparatus for flexible fluid delivery for cooling desired hot spots in a heat producing device," …2006.

[33] T. W. Kenny, M. Munch, P. Zhou, and J. G. Shook, "Patent US7000684 - Method and apparatus for efficient vertical fluid delivery for cooling a ... - Google Patents," …2006.

[34] S. Narayanan, A. G. Fedorov, and Y. K. Joshi, "Experimental characterization of a micro-scale thin film evaporative cooling device," pp. 1–10, May 2010.

[35] R. S. Prasher, J.-Y. Chang, I. Sauciuc, S. Narasimhan, D. Chau, G. Chrysler, A. Myers, S. Prstic, and C. Hu, "Nano and Micro Technology-Based Next-Generation Package-Level Cooling Solutions," Intel Technology Journal, vol. 9, no. 4, pp. 285–296, Jan. 2005.

[36] A. Koşar, C.-J. Kuo, and Y. Peles, "Boiling heat transfer in rectangular microchannels with reentrant cavities," International Journal of Heat and Mass Transfer, vol. 48, no. 23, pp. 4867–4886, Nov. 2005.

[37] J. Weibel and S. Garimella, " Visualization of vapor formation regimes during capillary-fed boiling in sintered-powder heat pipe wicks," International Journal of Heat and Mass Transfer 55, pp. 3498–3510, 2012.

[38] N. Miljkovic, R. Enright, and E. N. Wang, "Effect of Droplet Morphology on Growth Dynamics and Heat Transfer during Condensation on Superhydrophobic Nanostructured Surfaces," ACS nano, vol. 6, no. 2, pp. 1776–1785, Feb. 2012.

[39] X. Dai, X. Huang, F. Yang, X. Li, J. Sightler, Y. Yang, and C. Li, "Enhanced nucleate boiling on horizontal hydrophobic-hydrophilic carbon nanotube coatings," Applied Physics Letters, vol. 102, no. 16, p. 161605, 2013.

[40] Z. Yao, "Pool Boiling Heat Transfer Enhancement Through Nanostructures on Silicon Microchannels," J. Nanotechnol. Eng. Med., vol. 3, no. 3, p. 031002, Aug. 2012.

[41] K. E. Goodson, K. Kurabayashi, and R. F. W. Pease, "Improved heat sinking for laser-diode arrays using microchannels in CVD diamond," Components, Packaging, and Manufacturing Technology, Part B: Advanced Packaging, IEEE Transactions on, vol. 20, no. 1, pp. 104–109, 1997.